

of MIL-88B and MIL-88D (fig. S9). Unlike MIL-88C, the plane of the rings in the other members points toward the interior of the tunnel and leaves less room for adsorption, especially for MIL-88D. When starting from the dried form, the pore opening remains rather weak (<20%) when the solid is dispersed at room temperature in a liquid, despite the importance of the organic linker (fig. S10). Alternatively, the use of the as-synthesized form of MIL-88D leads to an almost MIL-88B-like adsorption behavior (figs. S11 and S12); with adsorption of different liquids, the magnitude of pore opening depends, once more, on the nature of the guest. Besides the specific interactions between solvent molecules and the framework, a geometrical threshold exists for an adsorption in the tunnels. Moreover, this threshold is thermally activated, because at 150°C, dispersion of MIL-88D in pyridine leads to its total opening (fig. S13). The same behavior is observed for MIL-88C in its dried state. Dispersed in DMF at room temperature, it exhibited a 60% pore opening, whereas the same experiment performed at 150°C showed a total opening (170%) (fig. S14). However, thermodynamically, if there is a thermal effect related to the pore opening of the framework, it is masked by that of solvation, which occurs simultaneously.

We can briefly discuss the kinetics of adsorption. From our experiments, it seems that the kinetics of breathing is distinctive for each MIL-88-solvent association. For example, MIL-88A and MIL-88B breathe within a few seconds in the presence of ethanol, whereas it takes several days for MIL-88B to open its pores completely in the

presence of water or nitrobenzene (figs. S15 and S16). Similarly, MIL-88C opens rapidly with pyridine (<1 min) but slowly with DEF (hours).

Finally, it is not known whether there is a phase transition when a solvent is adsorbed. The nets are topologically invariant and are not reconstructed between the different forms. In this sense, if there is a transition, it might be only a displacement, but even in this case, most of the structural transitions are associated with a change in symmetry and, therefore, in the XRD patterns. Here, the space group remains the same ( $P-62c$  or  $P6_3/mmc$ ), and the patterns show a continuous evolution (figs. S17 to S20). Thus, this breathing phenomenon is reversible for each solid and without any apparent loss of crystallinity, even if anisotropic peak broadening is observed with drying for the (hk0) Bragg reflections while (001) peaks retain their initial width. However, the anisotropy disappears with wetting, and both (hk0) and (001) reflections recover the same peak width, which also rules out the appearance of an impurity or a structural change during the breathing phenomenon. At first glance, the peak broadening with drying could be due to some disorder (residual molecules of solvent) in the (ab) plane.

The cyclability of the breathing phenomenon has not been addressed so far. However, we have observed by XRD that the pore opening still occurs with no apparent loss of crystallinity after a few desolvation-solvation cycles (fig. S17 to S20). Further investigations will be needed in order to understand both the energetics and the cyclability of this breathing phenomenon.

## References and Notes

1. K. Barthelet, J. Marrot, D. Riou, G. Férey, *Angew. Chem. Int. Ed.* **41**, 281 (2002).
2. C. Serre *et al.*, *J. Am. Chem. Soc.* **124**, 13519 (2002).
3. S. Kitagawa, K. Uemura, *Chem. Soc. Rev.* **34**, 109 (2005).
4. A. J. Fletcher, K. Thomas, M. Rosseinsky, *J. Solid State Chem.* **178**, 2491 (2005).
5. K. Uemura, R. Matsuda, S. Kitagawa, *J. Solid State Chem.* **178**, 2420 (2005).
6. C. Serre, F. Millange, S. Surblé, G. Férey, *Angew. Chem. Int. Ed.* **43**, 6285 (2004).
7. C. Mellot-Draznieks, J. Dutour, G. Férey, *Angew. Chem. Int. Ed.* **43**, 6290 (2004).
8. G. Férey *et al.*, *Angew. Chem. Int. Ed.* **43**, 6296 (2004).
9. G. Férey *et al.*, *Science* **309**, 2040 (2005).
10. S. Surblé, C. Serre, C. Mellot-Draznieks, F. Millange, G. Férey, *Chem. Commun.* **2006**, 284 (2006).
11. C. Mellot-Draznieks *et al.*, *J. Am. Chem. Soc.* **127**, 16273 (2005).
12. Supplementary data and figures are available on Science Online.
13. We are indebted to the ESRF in Grenoble for providing beamtime and for the help of the staff during and after the experiments. F. Millange and G. Marsolier are also acknowledged for their help in collecting XRD patterns. CNRS is acknowledged for financial support. Coordinates of MIL-88A to D deduced from computer simulation (dry, open forms) as well as the experimental structures of the open forms of MIL-88A to D (with solvents) have been deposited with ICSD data bank, deposition numbers CSD 417746, 417747, 417748, 417749, 417750, 417751, 417752, 417753, 417756, 417757, 417758, and 417759.

## Supporting Online Material

[www.sciencemag.org/cgi/content/full/315/5820/1828/DC1](http://www.sciencemag.org/cgi/content/full/315/5820/1828/DC1)

Materials and Methods

Figs. S1 to S20

Table S1

References

27 November 2006; accepted 21 February 2007

10.1126/science.1137975

# Plastic Deformation Recovery in Freestanding Nanocrystalline Aluminum and Gold Thin Films

Jagannathan Rajagopalan, Jong H. Han, M. Taher A. Saif\*

In nanocrystalline metals, lack of intragranular dislocation sources leads to plastic deformation mechanisms that substantially differ from those in coarse-grained metals. However, irrespective of grain size, plastic deformation is considered irrecoverable. We show experimentally that plastically deformed nanocrystalline aluminum and gold films with grain sizes of 65 nanometers and 50 nanometers, respectively, recovered a substantial fraction (50 to 100%) of plastic strain after unloading. This recovery was time dependent and was expedited at higher temperatures. Furthermore, the stress-strain characteristics during the next loading remained almost unchanged when strain recovery was complete. These observations in two dissimilar face-centered cubic metals suggest that strain recovery might be characteristic of other metals with similar grain sizes and crystalline packing.

In coarse-grained metals, dislocation-mediated processes govern plastic deformation, with the dislocations generated by intragranular sources. Dislocations propagating in intersecting slip planes can interact with each other and, in the process, form new dislocations that are immobile. These immobile dislocations obstruct the passage of other slip dislocations through these planes

and harden the crystal, a phenomenon commonly referred to as work hardening (1).

Nanocrystalline metals, where the grain size is typically less than 100 nm, are expected to behave differently because the grain size is smaller than the characteristic length scales associated with nucleation and propagation of dislocations (2–4). Experiments (5, 6) indicate that intragranular

dislocation sources like the Frank-Read source cease to operate in nanocrystalline metals, although in situ transmission electron microscopy (TEM) observations of tensile deformation have shown dislocation activity, especially near crack tips (7). The lack of dislocation sources results in high strength and reduced plasticity in these materials (8, 9), although recent experiments (10) indicated that stress-assisted grain growth during deformation can lead to enhanced ductility. Atomistic simulations suggest that dislocations nucleated at grain boundaries (GBs) carry out plastic deformation in the nanocrystalline regime; once nucleated, these dislocations travel across the grains and are eventually absorbed in the opposite GB (11–13). Atomistic simulations and experiments also suggest that, at very small grain sizes (~10 nm), GB sliding and migration become the dominant deformation mechanisms and cause a reduction in strength (14–17).

Although the behavior of nanocrystalline metals during deformation has been investigated, their postdeformation behavior has received little

Department of Mechanical Science and Engineering, University of Illinois at Urbana-Champaign, Urbana, IL 61801, USA.

\*To whom correspondence should be addressed. E-mail: saif@uiuc.edu

attention. We report an unexpected recovery of plastic deformation in sputter-deposited freestanding aluminum and gold films after unloading. Six aluminum specimens from two different wafers (batches) and two gold specimens from a single wafer were tested for this study, all of which showed plastic deformation recovery. The aluminum films were 200 nm thick, 50 to 60  $\mu\text{m}$  wide, and 300 to 360  $\mu\text{m}$  long; whereas the gold films were 200 nm thick, 12 to 20  $\mu\text{m}$  wide, and 185  $\mu\text{m}$  long. TEM observations and cross-sectional scanning electron microscopy (SEM) studies revealed an average grain size of 65 nm for the aluminum films. TEM observations, x-ray diffraction analysis, and cross-sectional SEM studies of the gold films revealed a strong [111] texture along the film growth direction and a mean grain size of 50 nm. The aluminum films typically had two to three grains along the film thickness (aspect ratio of 1 to 1.5), whereas the gold films had three to four grains (aspect ratio of 1 to 1.3). The specimens were macroscopically stress-free during the strain recovery, and the aluminum specimens showed strain recovery even at room temperature (RT), with the recovery rate increasing with increasing annealing temperature.

The freestanding aluminum and gold specimens were cofabricated with a microelectromechanical system-based tensile testing chip capable of measuring stress and strain simultaneously. This tensile testing chip is similar to the microtensile stage described in (18); the only difference is that the films in this case are deposited on Si and not SiO<sub>2</sub>. The chip is loaded by a piezo actuator that has a displacement resolution of 0.02  $\mu\text{m}$ , and the entire setup is placed in a scanning electron microscope for testing (19). The strain and stress resolution were 0.005% and 10 MPa, respectively, for measurements on the aluminum specimens. For the gold specimens, the corresponding values were 0.01% and 1.5 MPa.

We measured the stress-strain curves (Fig. 1) for a series of deformation recovery experiments performed on an aluminum specimen (specimen A). For all the experiments, the loading was performed at RT, and the annealing time was 7 min, except where indicated otherwise. The temperature fluctuation during annealing was less than  $\pm 2^\circ\text{C}$  for all the results reported. In the first

experiment (curve I), the specimen was deformed to 1.38% strain, inducing a plastic strain ( $\epsilon_p$ ) of 0.65%. During loading, the specimen started yielding around 330 MPa, where a marked reduction in the stress-strain slope (compared with 70 GPa in the elastic region) was seen. The specimen also showed strain hardening after yielding, as indicated by a positive, although reduced, postyielding slope. The stress-strain characteristics seemed to be time independent, because no stress relaxation or creep was seen when the piezo voltage was held constant for 5-min periods at various points during loading. This time independence was observed during all the subsequent loadings as well. However, fast relaxation processes, if any, could have gone undetected if they were occurring on time scales much shorter than our loading strain rate ( $\sim 1 \times 10^{-4} \text{ s}^{-1}$ ). The strain rate was obtained by observing the displacement of the sample ends directly (by using strain-sensing gauges, labeled G1 and G2 in fig. S1).

After rapid unloading (strain rate  $\sim 1 \times 10^{-3} \text{ s}^{-1}$ ), the specimen was annealed at 100°C for 15 min, which produced no noticeable recovery. The specimen was then annealed at 240°C for 7 min, during which time it recovered 0.33% strain ( $\sim 0.5\epsilon_p$ ). Annealing at 240°C for a further 20 min did not produce any additional recovery. In the second experiment (curve II), a plastic strain of 0.33% was induced so that the accumulated plastic strain was the same as after the first deformation. During loading, the stress-strain characteristics were almost identical to those of the first deformation, and the specimen recovered the entire additional plastic strain on annealing at 220°C.

Curve III shows the third loading and recovery (recoverable plastic strain  $\epsilon_{pr} = 0.52\%$ ) upon annealing at 205°C. Although the yield point remained unchanged, the specimen showed larger postyielding hardening as well as a larger fraction of recoverable plastic strain ( $\epsilon_{pr}/\epsilon_p \sim 0.7$ ) compared with the first experiment, which points to a link between work hardening and plastic deformation recovery. Further annealing at 240°C did not produce any additional recovery. The fourth and fifth experiments were performed to assess the temperature dependence of strain recovery; the annealing temperatures were 120°C and 60°C, respectively. Curves IV and V show that the

recovery at 120°C is substantially larger ( $\epsilon_{pr} = 0.4\%$ ) compared with that at 60°C ( $\epsilon_{pr} = 0.24\%$ ), even though the  $\epsilon_p$  is almost identical ( $\epsilon_p \sim 0.4\%$ ). During the sixth experiment (curve VI), the specimen showed notable residual work hardening as the yield stress increased to 395 MPa from 330 MPa. Moreover, a strain of 1% induced a plastic strain of only 0.23%, whereas in previous experiments the plastic strain was  $\sim 0.3\%$ . The specimen was then left at RT for 19 hours, during which time it recovered 0.25% strain. When the specimen was loaded from this point, the deformation path was similar to curve VI, confirming the presence of residual hardening in the absence of full recovery of  $\epsilon_{pr}$ . Upon annealing at 48°C, the specimen recovered 0.23% strain. In these experiments, the stress-strain measurements were done at fairly large increments of strain, because the stress-strain behavior of similar aluminum films had been well characterized in previous studies (20, 21). TEM observations of the specimen after deformation and annealing at 240°C did not reveal any noticeable change in the grain size compared to the as-fabricated state (fig. S2). The findings presented were certified by similar experiments on other aluminum specimens.

To verify whether plastic strain recovery occurs in other face-centered cubic (fcc) metals, we performed similar experiments (19) on gold films synthesized by using the same technique. The gold specimens, like the aluminum specimens, showed no stress relaxation or creep during loading in any of the experiments. Figure 2 shows the strain recovery measurements on one of the gold specimens. In the first experiment, the specimen was deformed to 1.28% strain, leading to a plastic strain of 0.7%. During loading, the specimen started yielding at around 70 MPa and showed substantial postyielding hardening. After unloading, the specimen showed no strain recovery when annealed at 100°C for 10 min but recovered 0.35% strain ( $0.5\epsilon_p$ ) after annealing at 210°C for 5 min. Further annealing at 210°C did not result in any additional recovery. When the specimen was loaded again, the stress-strain characteristics were very similar to the first loading. TEM observations showed no grain growth during either deformation or annealing.

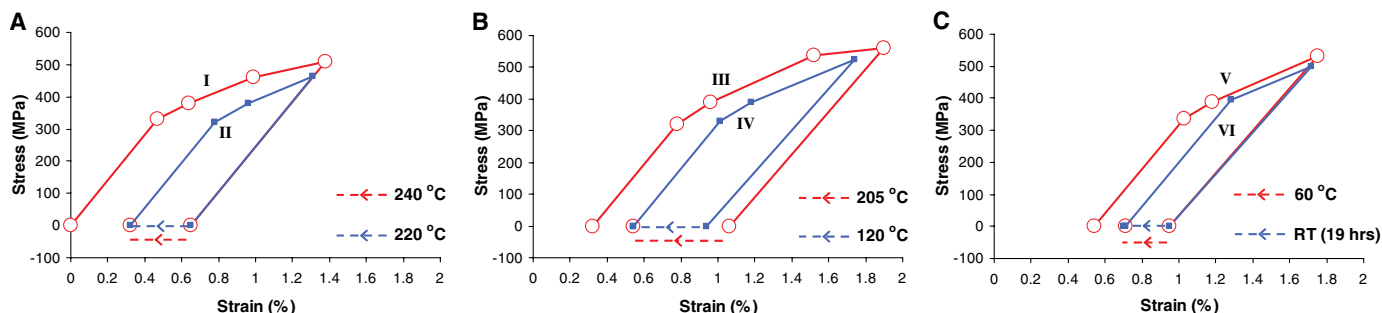


**Fig. 1.** (A to C) Stress-strain curves for deformation recovery experiments on specimen A (aluminum). A fraction of the plastic strain is recoverable, and, once that strain is recovered, the specimen shows no residual hardening

during the next loading. When recovery is incomplete (curve V), an increase in yield stress is seen during the next loading (curve VI). The dashed arrows indicate strain recovery at different annealing temperatures.

In a thermally activated process, one would expect to see a substantial drop in the rate with a reduction in temperature. But in the aluminum specimen (specimen A), annealing at 60°C and 48°C produced very similar amounts of strain recovery, whereas the recovery at 120°C was substantially higher. This suggests that a fraction of strain recovery, possibly involving higher activation energy processes, is accessible only at high temperatures (>100°C) within the 7-min annealing time. To test this hypothesis, we annealed a similar aluminum specimen (specimen B) at 240°C a priori and then deformed it to a plastic strain of 0.55%. We then observed the time dependence of recovery at different annealing temperatures (Fig. 3). The results indicate that a fraction of RT recovery (~40%) occurs very quickly, within a time period of about 400 s, whereas processes that are much slower (time constant ~ 10<sup>5</sup> s) dictate the rest of the recovery. Also, increasing the temperature leads to sharp spurts in recovery that saturate in a short period of time. These observations suggest that the recovery process is governed by a distribution of activation energies and that higher temperatures help to overcome larger activation barriers faster.

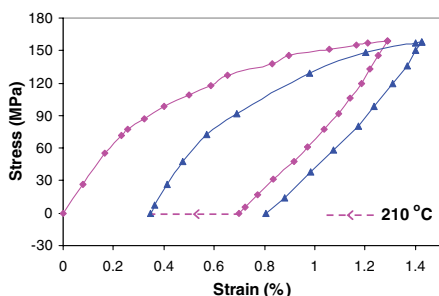


**Fig. 2.** Stress-strain curves for deformation recovery experiments performed on a gold specimen. This specimen also showed substantial (50%) plastic strain recovery and no residual hardening during the next loading.

Because both the aluminum and gold films were sputter-deposited and had similar grain sizes, we performed the same experiment on two sputter-deposited aluminum films of similar thickness (215 nm) but with a much larger average grain size (180 nm) to check whether the strain recovery is restricted to certain range of grain sizes. These films were also annealed a priori at 240°C and then deformed to a plastic strain of 0.55%. However, these films showed no deformation recovery even when annealed at 220°C for 30 min. This observation and the fact that similarly synthesized aluminum films, but with much smaller grain sizes (10 to 20 nm), show very little plasticity during deformation (22) suggest that the strain recovery is restricted to a small range of grain sizes. We noted, however, that the large-grained (180 nm) aluminum films had a columnar grain structure, unlike the films that showed recovery, which could have also caused them to behave differently.

The experimental results reveal that the deformation recovery is time dependent and that the process is thermally activated. Because the specimens are macroscopically stress-free when the recovery occurs, it is likely that this process is driven by residual internal stresses caused, perhaps, by inhomogeneous deformation during loading. Figure 4A shows an energy landscape that could govern the loading and unloading processes. During the initial stages of loading, all

the grains deform elastically, leading to homogeneous elastic deformation strain ( $\epsilon_e$ ). After a critical stress (the macroscopic yield point) is reached, some relatively larger or favorably oriented grains start deforming plastically, whereas others still accommodate the strain elastically. This leads to increased compliance and hence a reduced but positive stress-strain slope. During this phase, plastic deformation proceeds with the overcoming of local energy barriers. However, due to the inhomogeneous nature of the deformation, internal stresses build up in the specimen. As the external stress is increased, even relatively smaller or unfavorably oriented grains start deforming plastically, eventually leading to homogeneous plastic deformation with near-zero stress-strain slope. The plastic strain in the specimen hence is composed of permanent plastic strain ( $\epsilon_{pp}$ ), resulting from homogeneous deformation (no internal stress buildup), and recoverable plastic strain ( $\epsilon_{pr}$ ), which occurs during inhomogeneous deformation.

On unloading,  $\epsilon_e$  is instantaneously recoverable, whereas  $\epsilon_{pp}$  is completely irrecoverable.  $\epsilon_{pr}$  recovers over time, driven by the reduction in internal residual stresses. Because this process involves the overcoming of local energy barriers, it exhibits temperature dependence as well. It is quite likely that the apparent strain hardening seen during loading in our experiments on both

**Fig. 3.** Time evolution of strain recovery at different annealing temperatures for specimen B (aluminum). About 40% of strain recovery at RT happens within 400 s, whereas the rest of the recovery takes much longer time. The sharp spurts in recovery after increasing the temperature saturate in a short period of time. These characteristics of the strain recovery indicate that it is thermally activated and that it may involve a distribution of activation energies.

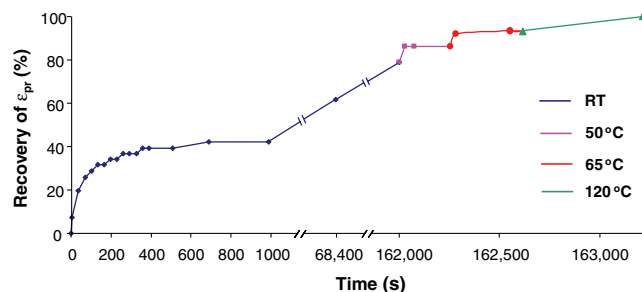
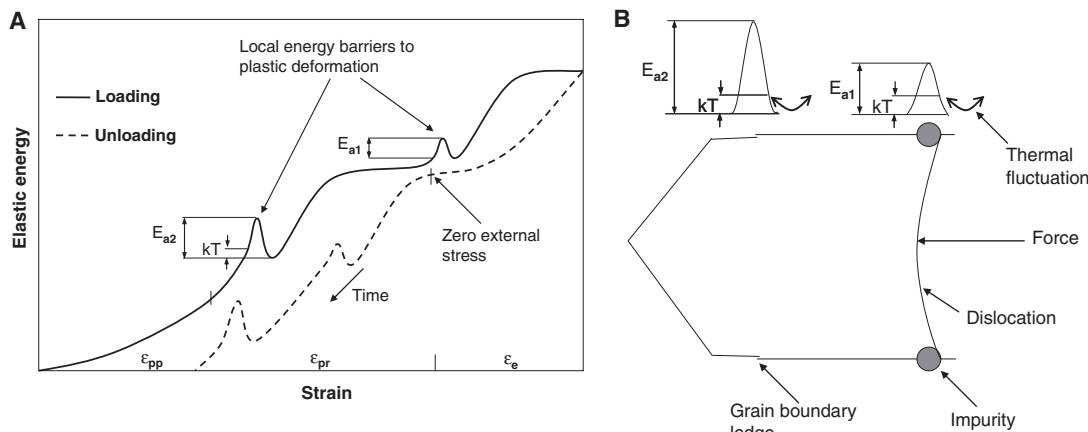


**Fig. 4. (A)** Energy landscape for loading and unloading. During loading, the strain is composed of homogenous elastic strain ( $\epsilon_e$ ), permanent plastic strain ( $\epsilon_{pp}$ ), and recoverable plastic strain ( $\epsilon_{pr}$ ). On unloading,  $\epsilon_e$  is instantaneously recoverable, and  $\epsilon_{pp}$  is completely irrecoverable, whereas  $\epsilon_{pr}$  recovers over time.  $\epsilon_e$ ,  $\epsilon_{pr}$ , and  $\epsilon_{pp}$  shown are for the unloading process. **(B)** Dynamics of dislocation glide. The dislocation is pinned at the ends by GB defects that act as barriers to its propagation during both loading and unloading. Depinning occurs through local atomic rearrangements arising from thermal fluctuations and leads to further propagation. During loading, the dislocation experiences



a force due to the external applied stress, whereas after unloading the force arises from residual internal stresses caused by inhomogeneous deformation.

aluminum and gold is a result of inhomogeneous deformation that encompasses  $\epsilon_{pr}$ . It would also explain why larger strain hardening leads to a larger fraction of recoverable strain, as seen during the third experiment on the aluminum sample (Fig. 1B, curve III). In the figure,  $\epsilon_{pr}$  and  $\epsilon_{pp}$  are shown separately for the loading process merely to enhance clarity; these processes can occur simultaneously.

A process that can lead to this kind of strain recovery can be visualized as follows. Consider a dislocation that has moved into the grain interior because of applied stress (Fig. 4B). The dislocation is pinned at the ends by GB defects that act as barriers to its propagation during both loading and unloading. During loading, the large external stress along with the thermal fluctuations allows the dislocation to overcome the barriers quickly. At a given stress, once a barrier is overcome, the dislocation attains equilibrium, because further propagation would involve an “uphill ride,” that is, an increase in energy due to the positive slope of the energy landscape. During strain recovery after unloading, the residual internal stresses drive the dislocation back to the GB where it originated. But, unlike loading, the reverse motion of the dislocation involves a “downhill ride” along the energy landscape, and hence it continues to move backward through thermally assisted depinning until all the residual stresses are eliminated.

Atomistic simulations (23) have shown that GB ledges, which act as pinning points, could hinder dislocation propagation and that depinning occurs through thermal activation, leading to further propagation. Some experimental studies (24, 25) have also provided indirect evidence for such a mechanism. It is quite conceivable that such dislocation pinning and thermally activated depinning is responsible for the temperature dependence of recovery rate seen in our experiments, where, apart from GB ledges, impurities present in the GBs could also act as pinning points. To assess the impurity levels in the samples, we examined them in as-fabricated as well as annealed condition by using Auger electron spectroscopy. Both the as-fabricated and annealed aluminum films (fig. S3) showed similar impurity levels, with a fairly large nitrogen content (~4.5%) and smaller amounts of carbon and oxygen (<1% each). Similarly, there was no major difference in the impurity contents of as-fabricated and annealed gold samples, but both of them had much less nitrogen content (<0.5%) compared with the aluminum films. In assessing the possibility of impurities acting as pinning points, it is worth noting that, although specimen A did not show any noticeable recovery at 100°C during the first experiment, it recovered even at 48°C, after it had undergone annealing at 240°C. This enhancement of recovery rate could be due to the reduction in pinning sites caused by redistribution of GB impurities during high temperature annealing.

The process described in Fig. 4B is just one possible strain recovery mechanism. One can visualize such thermally assisted strain recovery

for plastic deformation resulting from other processes, like diffusion-assisted GB sliding and grain rotation. For example, it has been shown that an internal stress field with cracklike singular stresses can develop when GB diffusion is blocked by an obstacle in a thin film (26–29). Hence, if diffusivity is not uniform in all GBs in a thin film, either because of presence of impurities or because of inherent variations in the structure of GBs, deformation will result in heterogeneous GB diffusion. Such diffusion can cause severe internal stresses to develop during loading that can serve as driving force for plastic strain recovery.

Although there have been no previous reports of substantial (50 to 100%) plastic strain recovery in nanocrystalline materials, investigations on bulk nanocrystalline Ni (30, 31) have revealed that x-ray peak broadening due to inhomogeneous strain during loading is reversible upon unloading at RT but not at 180 K and that the additional broadening at 180 K disappears on warming to RT. Furthermore, time-dependent recovery of root mean square strain (32) and existence of small negative creep (~2% of total plastic strain) during strain dip tests (24) have also been reported for bulk nanocrystalline Ni. These results, along with our observation of thermally activated strain recovery in thin films, suggest that there is a substantial thermal component and an element of reversibility in plastic deformation of nanocrystalline fcc metals, in both bulk and thin film form.

Although both gold and aluminum are free metals, some of their properties, such as stacking fault energy (30 mJ m<sup>-2</sup> for gold, 120 mJ m<sup>-2</sup> for aluminum), differ substantially. Furthermore, the gold films tested in this study differ from aluminum films in the following aspects: (i) absence of native oxide layer on the surface, (ii) presence of strong [111] texture along the film growth direction, and (iii) smaller impurity content. Despite these differences, they show similar strain recovery characteristics, which suggests that grain size dictates strain recovery. Hence, it is reasonable to expect similar behavior in other fcc metals if they have similar grain sizes.

The experimental observations suggest that strain recovery results from the combined effect of a small mean grain size and inhomogeneities in the microstructure (variations in the size and orientation of individual grains and structure of GBs); the small grain size precludes intragranular dislocation sources, whereas variations in the microstructure lead to plastic deformation (through dislocations originating from GBs) in relatively larger grains and elastic accommodation in smaller grains. Upon unloading, this results in inhomogeneous residual internal stresses, which drive the strain recovery. Hence, in exploring plastic deformation of nanocrystalline metals, it might be necessary to consider not only the average size of the microstructure but also the inherent variations.

## References and Notes

1. A. H. Cottrell, *Dislocations and Plastic Flow in Crystals* (Oxford Univ. Press, Oxford, 1953).
2. E. Arzt, *Acta Mater.* **46**, 5611 (1998).
3. S. P. Baker, *Mater. Sci. Eng. A* **319–321**, 16 (2001).
4. J. R. Weertman, in *Nanostructured Materials: Processing, Properties, and Applications*, C. C. Koch, Ed. (William Andrews, Norwich, NY, 2002).
5. M. Legros, B. R. Elliot, M. N. Rittner, J. R. Weertman, K. J. Hemker, *Philos. Mag. A* **80**, 1017 (2000).
6. M. A. Haque, M. T. A. Saif, *J. Mater. Res.* **20**, 1769 (2005).
7. K. S. Kumar, S. Suresh, M. F. Chisholm, J. A. Horton, P. Wang, *Acta Mater.* **51**, 387 (2003).
8. M. A. Haque, M. T. A. Saif, *Sens. Actuators A* **97–98**, 239 (2002).
9. Y. M. Wang *et al.*, *Scr. Mater.* **48**, 1581 (2003).
10. D. S. Gianola *et al.*, *Acta Mater.* **54**, 2253 (2006).
11. V. Yamakov, D. Wolf, S. R. Phillpot, A. K. Mukherjee, H. Gleiter, *Nat. Mater.* **1**, 45 (2002).
12. J. Schiøtz, K. W. Jacobsen, *Science* **301**, 1357 (2003).
13. H. Van Swygenhoven, P. M. Derlet, A. Hasnaoui, *Phys. Rev. B* **66**, 024101 (2002).
14. J. Schiøtz, F. D. Tolla, K. W. Jacobsen, *Nature* **391**, 561 (1998).
15. V. Yamakov, D. Wolf, S. R. Phillpot, A. K. Mukherjee, H. Gleiter, *Nat. Mater.* **3**, 43 (2004).
16. H. Conrad, J. Narayan, *Appl. Phys. Lett.* **81**, 2241 (2002).
17. K. J. Van Vliet, S. Tsikata, S. Suresh, *Appl. Phys. Lett.* **83**, 1441 (2003).
18. J. H. Han, M. T. A. Saif, *Rev. Sci. Instrum.* **77**, 045102 (2006).
19. Materials and methods are available as supporting material on *Science Online*.
20. M. A. Haque, M. T. A. Saif, *Acta Mater.* **51**, 3053 (2003).
21. M. A. Haque, M. T. A. Saif, *Proc. Natl. Acad. Sci. U.S.A.* **101**, 6335 (2004).
22. M. A. Haque, M. T. A. Saif, *Scr. Mater.* **47**, 863 (2002).
23. H. Van Swygenhoven, P. M. Derlet, A. G. Froseth, *Acta Mater.* **54**, 1975 (2006).
24. S. Van Petegem, S. Brandstetter, H. Van Swygenhoven, J.-L. Martin, *Appl. Phys. Lett.* **89**, 073102 (2006).
25. Y. M. Wang, A. V. Hamza, E. Ma, *Acta Mater.* **54**, 2715 (2006).
26. H. Gao, L. Zhang, W. D. Nix, C. V. Thompson, E. Arzt, *Acta Mater.* **47**, 2865 (1999).
27. D. Weiss, H. Gao, E. Arzt, *Acta Mater.* **49**, 2395 (2001).
28. M. J. Buehler, A. Hartmaier, H. Gao, *J. Mech. Phys. Solids* **51**, 2105 (2003).
29. A. Hartmaier, M. J. Buehler, H. Gao, *Mater. Sci. Eng. A* **400–401**, 260 (2005).
30. Z. Budrovic, H. Van Swygenhoven, P. M. Derlet, S. Van Petegem, B. Schmitt, *Science* **304**, 273 (2004).
31. S. Brandstetter *et al.*, *Appl. Phys. Lett.* **87**, 231910 (2005).
32. S. Brandstetter *et al.*, *Adv. Mater.* **18**, 1545 (2006).
33. Supported by NSF grants ECS 05-24675 and ECS 03-04243 and Air Force Office of Scientific Research grant USAF-5212-STI-SC-0004. The x-ray diffraction and Auger spectroscopy measurements were carried out in the Center for Microanalysis of Materials, University of Illinois (UIUC), which is partially supported by the U.S. Department of Energy under grant DEFG02-91-ER45439. The tensile testing stage was fabricated in the Micro-Miniature Systems Laboratory and the Micro-Nano Technology Laboratory at UIUC. Experiments were performed in the environmental SEM at the Beckman Institute at UIUC. We thank W. D. Nix (Stanford University), F. Spaepen (Harvard University), and G. Dehm (Erich Schmid Institute of Materials Science) for valuable discussions.

## Supporting Online Material

www.sciencemag.org/cgi/content/full/315/5820/1831/DC1  
Materials and Methods  
Figs. S1 to S3

14 November 2006; accepted 26 February 2007  
10.1126/science.1137580